Production Engineering (2026) 20:22
https://doi.org/10.1007/s11740-025-01402-6

ORIGINAL PAPER

Manufacturing multi-material ceramics by sinterjoining based on vat photopolymerization (VPP)

Johannes Schubert[1] · **Michael Schott**[1] · **Frederik Zanger**[1]

Received: 1 September 2025 / Accepted: 2 December 2025 / Published online: 17 December 2025

Abstract

The combination of different ceramic materials within one component enables the targeted adjustment of material properties, allowing for enhanced performance, improved mechanical characteristics, and tailored functionality to meet specific application requirements. One promising approach for combining ceramic components is sinterjoining, where components with different shrinkage behaviors in the green or brown state are inserted into each other, forming a cohesive bond during the subsequent sintering process. In the present work, the sinterjoining approach was investigated for producing material composites from parts produced by vat photopolymerization. To do so, the shrinkage behavior of different ceramic materials of the material system Al_2O_3 – ZrO_2 was analyzed by dilatometric analysis. In an experimental study, the influence of the sintering conditions on the material properties of several materials of the system Al_2O_3 – ZrO_2 was investigated to derive suitable sintering conditions for a co-sintering of different materials. Sintering at 1650 °C for 2 h was identified as good compromise, leading to densities of more than 93 % for all materials considered and material-dependent hardness values between 1150 and 1500 HV2. The results were initially used for a monolithic sinterjoining approach, i.e., the combination of the same material but with different volume shrinkage in one component. For dimensioning, a factor $j_{sinterjoining}$ was defined, leading to suitable joining results of up to 99 % sintered boundary length ("Degree of Sintering"). Based on this, the joining of different materials of the system Al_2O_3 – ZrO_2 was investigated. Although multi-material sinterjoining is significantly more complex, good results have been achieved for various material combinations showing Degrees of Sintering of more than 95 % for several combinations. In particular, the combination of Al_2O_3 and an equal mass mixture of Al_2O_3 and ZrO_2 (AZ50) appears to be promising. The results demonstrate the potential of sinterjoining for producing ceramic composites and serve as a starting point for further optimizations.

Keywords Additive manufacturing · Ceramics · Sinterjoining · Multi-Material · Composites

1 Introduction

The use of additive manufacturing technologies, coupled with the capacity to meticulously adjust and tailor the properties of components to meet exacting specifications, enables the efficient and resource-efficient production of complex components from batch size one [1]. The integration of additive manufacturing with ceramic components offers a unique combination of the freedom and flexibility inherent in additive manufacturing processes with the exceptional mechanical properties and durability that ceramics are renowned for [2]. The demand for increased functionality in technical ceramic components is driving a requirement for innovative product solutions with enhanced functional density. A significant expansion of the achievable component properties and the underlying technical processes is the targeted combination of different ceramics in a single component [3].

Vat photopolymerization (VPP) is frequently used in research and industry for producing ceramic components due to its high manufacturing precision, the variety of technical ceramics that can be processed and the ability to produce ceramics with a high relative density of over 99 % [4, 5]. In the VPP process, a ceramic suspension comprising ceramic powder and an organic binder system is used. Aluminum oxide (alumina, Al_2O_3), zirconium oxide (zirconia, ZrO_2), and their

✉ Frederik Zanger
frederik.zanger@kit.edu

[1] wbk Institute of Production Science, Karlsruhe Institute of Technology (KIT), Kaiserstraße 12, Karlsruhe 76131, Germany

composites, i.e., alumina-toughened zirconia (ATZ) and zirconia-toughened alumina (ZTA), are frequently used materials in vat photopolymerization [6]. However, combining different ceramic materials in one component is still at the beginning of research due to the demanding requirements [7, 8].

Various joining methods for producing multi-ceramic components have been investigated [7]. One such approach is sinterjoining, where components with different shrinkage behaviors in the green ("as printed") or brown ("debinded") state are inserted into each other, forming a cohesive bond during the subsequent sintering process. A notable advantage of sinterjoining is that it does not require auxiliary materials for combining the materials, thereby eliminating restrictions imposed by conventional joining methods on the properties of the components [9].

However, sinterjoining of different VPP components is just barely investigated. In [9], a sinterjoining approach based on green parts having the same volume share and an interference fit was investigated. To create a clearance fit for inserting the parts into each other, a pre-sintering step was performed.

In [10], the mechanisms relevant for sinterjoining of MIM components for micro applications were theoretically analyzed. As key influencing factors, sintering time and temperature, particle geometry and size distribution, and the number of neighboring particles were identified. An experimental investigation showed that increasing the joining gap reduced the visual quality of the joint, though no significant impact on tensile strength was observed. Furthermore, general rules identified for conventional sintering seem to apply also for sinterjoining.

Sinterjoining of micro-injection molded ceramic parts from Al_2O_3 and ZrO_2 was analyzed in [11]. The work highlights the influence of thermal expansion coefficient and the material-dependent sintering shrinkage on the joining quality. Besides guaranteeing a larger volume shrinkage of the outer part, it must be prevented that a joining gap is created due to a higher thermal contraction of the inner part while cooling down after sintering.

In [12], dilatometric analyses of pressed ceramic specimens of Al_2O_3 and ZrO_2 were performed serving as data basis for subsequent analyses of the joining quality in sinterjoining. The results show that, as the sintering temperature increases, the clearance between the inner and outer parts decreases, thereby enhancing the joining quality.

A sinterjoining strategy for combining parts produced by VPP and material extrusion (MEX) using the same Al_2O_3 powder and a filler content of 50 vol.-% was derived in [13]. Pre-sintering of the inner (VPP) part at 1450 °C and the outer (MEX) part at 1100 °C created a defined clearance of approx. 11 %, allowing for mutual insertion of the parts. In a subsequent final sintering step at 1650 °C performed to achieve a press-fit connection. The joint interface remained partially visible in micrographs, so placement outside load-critical zones was recommended.

However, there is up to now no strategy for combining VPP parts without a pre-sintering step. Furthermore, no results regarding the combination of VPP parts of different materials are present.

The aim of the present study is to investigate the approach of sinterjoining for manufacturing multi-material ceramics. The investigation of sinterjoining and the production of multi-material components necessitates a thorough examination of the material-specific shrinkage behavior and the determination of optimized sintering parameters for multi-material components. Therefore, slurries with different ceramic filler contents are prepared, green parts were printed by VPP and debinded to brown parts. The shrinkage behavior of those brown parts was analyzed, enabling a sinterjoining approach of the same materials with different volume shrinkage. Based on these results, the combination of different materials is examined in a second step. The sinterjoining approach applied in this work is shown schematically in Fig. 1, based on [9].

2 Materials and methods

2.1 Raw materials

Ceramic suspensions for vat photopolymerization consist of ceramic powder and an organic binder system, which comprise an initiator system, matrix components and additives. Due to the favorable result, the binder components were adopted from [8]. This work was previously conducted by several authors of the present study and serves as a reference also in other parts of the paper to enable transferability of the results. In Table 1, details of the binder constituents used are shown. The selection of photoinitiators was based on the 460 nm wavelength of the VPP machine used. IBOA, HDDA, and ETMPTA serve as monomers with different functionalities leading to superior slurry properties. The Rheobyk additive was used to reduce the viscosity of the suspension.

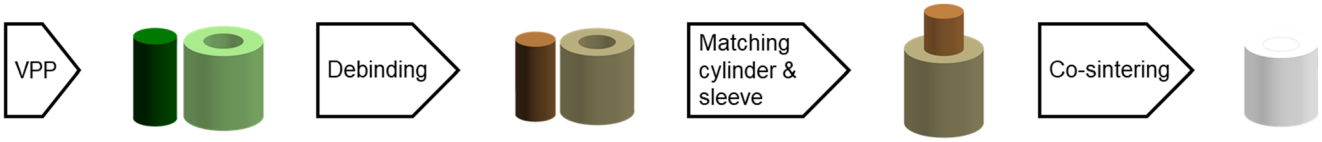

Fig. 1 Schematic visualization of the sinterjoining approach, based on [9]

Table 1 Overview of the organic substances used

Name	Supplier	Function
Isobornyl acrylate (IBOA)	TCI Chemicals	Monomer (1 functional group)
1,6-Hexanediol diacrylate (HDDA)	TCI Chemicals	Monomer (2 functional groups)
Trimethylolpropane ethoxylate triacrylate (ETMPTA)	TCI Chemicals	Monomer (3 functional groups)
Camphorquinone (CQ)	TCI Chemicals	Photoinitiator
4-(Dimethylamino) benzonitrile (4-DMA-BN)	TCI Chemicals	Co-initiator
Rheobyk	BYK-Chemie	Additive

The powders used were measured with regard to the percentile values of the agglomerate diameters using laser diffraction according to DIN ISO 13320:2022 [14] in a Sync (Microtrac Retsch, Haan, Germany). Furthermore, the particle size of the powders was determined using scanning electron microscopy JSM-6010 Plus (Jeol (Germany) GmbH, Freising, Deutschland). The specific surface of the powders was analyzed according to BET method described in DIN ISO 9277:2014 [15] by gas adsorption with nitrogen N_2 as adsorption gas. The results are shown in Table 2.

Based on the compelling results in [8], the slurry compositions used therein were largely taken over. For some materials a further increase of the ceramic content was possible based on iterative optimizations. The compositions used in the present work are summarized in Table 3. These values specify the highest possible ceramic content applicable with the corresponding binder composition up to now, i.e., 56 vol.-% for alumina and 50 vol.-% for zirconia and the composites thereof. For various test series within this work, the ceramic content was also reduced. To do so, the ceramic content was replaced by organic components in accordance with the composition of the remaining binder system.

Table 3 Summary of slurry compositions for various ceramic materials (in volume %)

Substance	Al_2O_3	ZTA	AZ50	ATZ	ZrO_2
IBOA	15.5	17.6	17.4	17.9	16.5
HDDA	15.5	17.5	17.3	17.7	16.4
ETMPTA	6.1	7.0	7.2	6.8	6.9
CQ	2.9	3.4	3.6	2.9	3.8
4-DMA-BN	0.9	1.1	1.3	1.4	1.4
Rheobyk	3.1	3.4	3.2	3.3	5.0
Ceramic	56.0	50.0	50.0	50.0	50.0

Table 4 Summary of the exposure parameters applied for the individual materials

Exposure parameters	Al_2O_3	ZTA	AZ50	ATZ	ZrO_2
Intensity in mW/cm²	80	80	80	80	80
Energy in mJ/cm²	70	80	85	95	105

2.2 Additive manufacturing of green parts

For producing the green parts, a vat photopolymerization machine CeraFab Multi 2M30 Science (Lithoz GmbH, Vienna, Austria) with a LED light source with 460 nm wavelength was used. Due to the nearly identical slurry compositions, the exposure parameters used in [8] were also applied in the present work. They are summarized in Table 4. Their applicability was verified by measuring the dimensions of cylindrical green parts analogously to [9] by a micrometer screw Micromar 40 ER (Mahr GmbH, Göttingen, Germany). Reference measurements were performed by a coordinate measuring machine Zeiss Prismo KMG (Carl Zeiss IQS Deutschland GmbH, Oberkochen, Germany) confirming the accuracy of the measurements performed by the micrometer screw.

2.3 Debinding

Based on the identical binder components of the slurries as used in [8], the same time-temperature profile was also used in the present work to transform the green parts into

Table 2 Overview of the ceramic and metal oxide powders used

Name	Supplier	Particle size in µm	Agglomerate size in µm			BET surface in $m^2 \cdot g^{-1}$
			d_{10}	d_{50}	d_{90}	
Al_2O_3	Final Advanced Materials GmbH, Freiburg, Germany	0.3	0.28	1.31	6.28	6.75
ZTA	*80/20 mixture by weight of Al_2O_3 and ZrO_2*					
AZ50	*50/50 mixture by weight of Al_2O_3 and ZrO_2*					
ATZ	*20/80 mixture by weight of Al_2O_3 and ZrO_2*					
ZrO_2	Tosoh Europe B.V., Amsterdam, Netherlands	0.2	0.31	0.97	2.55	5.39

debinded brown parts. This was determined in [8] on the basis of thermogravimetric analyses. The actual debinding takes place up to 455 °C, followed by a short heat-up to 1100 °C to increase the strength of the components enabling a handling of the components, as shown in Fig. 2. The debinding process was performed in a GLO 10/11 (Carbolite Gero, Neuhausen, Germany) in air atmosphere.

The roughness of the samples after debinding, i.e., the process stage in which cylinders and sleeves are inserted into each other, was determined on six randomly selected cylinders of varying materials and filler contents by perthometer measurements revealing arithmetic mean roughness values R_a ranging from 1.1 to 2.0 µm. Therefore, the values show that the roughness has no significant influence on the matching of cylinders and sleeves.

2.4 Determining shrinkage behavior and deriving sintering conditions

To investigate the material-specific shrinkage behavior during sintering as a basis for deriving suitable sintering conditions and for dimensioning the components for sinterjoining, an optical dilatometer TOMMI (Fraunhofer ISC, Würzburg, Germany) was used. Therefore, cylindrical samples with diameter 5 mm and height 10 mm were printed from slurries specified in Table 3 or from corresponding slurries with partially reduced filler content. They were debinded and pre-sintered up to 1100 °C for increasing their strength according to the temperature profile shown in Fig. 2. In the dilatometer, the samples were heated in air at 5 K/min to the maximum possible temperature of the measuring device of 1650 °C in accordance with DIN EN ISO 21821:2023 [16] and then held at this temperature for 120 min, while recording the lengths variations in horizontal and vertical direction. In a first test series, the shrinkage behavior of samples of different materials of the system Al_2O_3 – ZrO_2 was determined in dependency of the temperature. Similarly, the extent to which the filler content affects the shrinkage behavior was determined exemplarily for Al_2O_3 in a second test series.

For combining different materials in a single component, they have to undergo a common co-sintering process. Therefore, it is necessary to determine to what extent deviations from the typically applied sintering conditions affect the density and the mechanical properties of the materials. To identify suitable co-sintering conditions, cylindrical samples with 5 mm diameter and 10 mm height were printed and debinded analogous to the dilatometer samples. Based on the results of the dilatometric measurements and data sheet provided by Lithoz GmbH [17], an initial temperature profile shown in Table 5 was defined, whereby the sintering temperature was varied in 50 K steps between 1500 °C and 1700 °C and the dwell time between 2 h and 4 h in a test series. All sintering processes were performed in a HTF 18/4 chamber oven (Carbolite Gero GmbH & Co. KG, Neuhausen, Germany).

The density of the samples was determined according to DIN EN ISO 18754:2022 [18] using liquid displacement ("Archimedes") principle with an XSR204DR analytical balance with XPR/XSR-Ana density kit (both Mettler-Toledo GmbH, Giessen, Germany) after impregnating the samples using the boiling method for 1 h in distilled water as an immersion liquid.

Additionally, the samples were hot-embedded and prepared with various grinding disks up to grain size 1200. Vickers hardness measurements were carried out on the

Table 5 Time-temperature-profile for sintering the samples

Heating time in hh: mm	Heating rate in K/min	Target temperature in °C	Dwell time in h
		25	
00:58	1.3	100	0.0
08:20	2.0	1100	0.0
various	1.0	1500 – 1700	2.0 – 4.0
various	−1.0	1100	0.0
08:58	−2.0	25	0.0

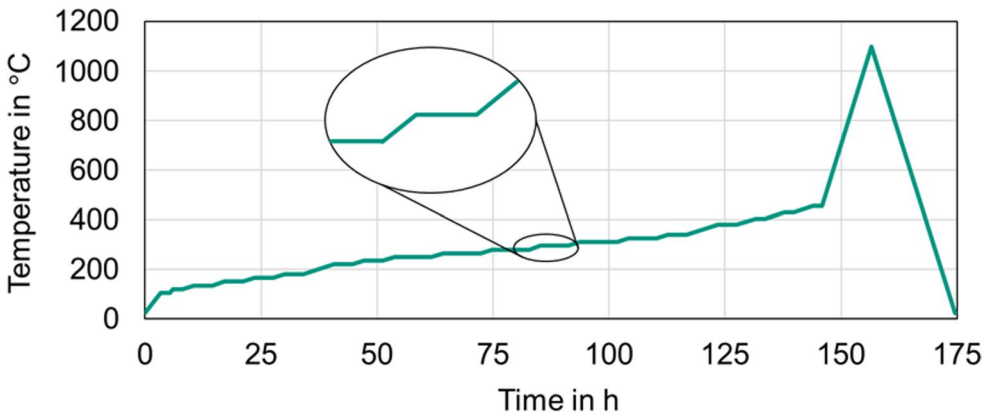

Fig. 2 Time-temperature-profile applied for debinding the green parts [8]

samples in accordance with DIN EN ISO 14705:2021 [19] using a Q10A + hardness tester (ATM Qness GmbH, Mammelzen, Germany) to HV 2.

In a further set of experiments, disk-shape samples with diameter 18 mm and thickness 1.8 mm in green state were printed from the five materials described above. After debinding and sintering, these were subjected to B3B tests to analyze their strength on a universal test machine UTS 10 (Karlsruhe Institute of Technology, Karlsruhe, Germany) with 8 mm hardened steel balls, allowing a reliable determination of the strength of brittle materials, esp. ceramics, also in the as-sintered state under a well-defined biaxial stress state with reduced errors due to misalignment and manufacturing tolerances. The support radius $r_{B3B,support}$ was calculated according to [20] from the radius of the support balls $r_{B3B,balls}$ using Formula 1

$$r_{B3B,support} = \frac{2\sqrt{3}}{3} \cdot r_{B3B,balls} \tag{1}$$

Following [21], the disk thickness $t_{B3B,disk}$ was determined in the center of the samples using a Micromar 40 ER micrometer (Mahr GmbH, Göttingen, Germany). For further evaluation, commonly accepted diagrams from [20, 22] were used to determine the factor f_{B3B} based on the geometric conditions. The maximum tensile stress in the disk $\sigma_{B3B,max}$ results from the disk thickness $t_{B3B,disk}$, the disk radius $r_{B3B,disk}$, the support radius $r_{B3B,support}$, the material-dependent Poisson's ratio ν, the factor f_{B3B} and the applied force F_{B3B} according to Formula 2.

$$\sigma_{B3B,max} = f_{B3B}\left(\frac{t_{B3B,disk}}{r_{B3B,disk}}, \frac{r_{B3B,disk}}{r_{B3B,support}}, \nu\right) \cdot \frac{F_{B3B}}{{t_{B3B,disk}}^2} \tag{2}$$

The evaluation was carried out using the Weibull approach according to DIN EN ISO 20501:2023 [23] by calculating the probability of failure of the specimen P_f in dependency of the load applied. Based on this, the characteristic strength σ_θ of the samples, being defined as the strength at P_f = 63.2 %, was calculated.

2.5 Sinterjoining

For investigating the sinterjoining approach, sleeves and cylinders with a height of 5 mm were used as test specimen. The outer diameter of the cylinders was set to be constantly 5 mm. The inner diameter of the sleeves used for monolithic sinterjoining in the first test series was varied in 14 steps between 5.00 mm and 5.88 mm. The step size between 5.00 mm and 5.16 mm was set to be 40 µm, while a larger step size of 80 µm was used between 5.16 mm and 5.88 mm. The utilization of a variable step size facilitates the exploration of a comprehensive parameter range, while ensuring the attainment of the highest attainable resolution within the presumably most pertinent range. The outer diameter of the sleeves was set to be constantly 10 mm. Those samples were used for the first set of experiments analyzing monolithic sinterjoining, i.e., the combination of cylinders and sleeves of the same material, and for the second set of experiments addressing multi-material sinterjoining. In the second set of experiments, cylinders and sleeves of different material of the material system Al_2O_3 – ZrO_2 were used. They were selected based on the results of the dilatometric analysis.

After debinding the samples according to Chap. 2.3, cylinders and sleeves of all dimensions described above were combined full-factorially by inserting the cylinders into the sleeve. It was documented whether the cylinders and sleeves could be placed into each other without additional force besides gravity, whether manual forces were required or whether joining was not possible at all. Subsequent to co-sintering using the best sintering parameters determined according to Chap. 2.4, the joined samples were hot-embedded and 2 mm of the sample height was ground-off to assess the joining quality in the center volume of the component and to avoid any influence on the samples by the introduction slopes. The interface between the two joining partners was then examined microscopically on a XM420 (Wild Heerbrugg AG, Heerbrugg, Switzerland) and the software PRECiV Core (Evident Corporation, Tokyo, Japan). For assessing the joining quality, the Degree of Sintering (DoS) measure was used, as defined by [9]. For cylindrical components, i.e. circular interfaces, the Degree of Sintering can either be derived based on the length or the circumference or the angle enclosed by the sintered sections α_i. Hence, the Degree of Sintering is defined as share of the sintered interface in comparison to the initial interface between cylinder and sleeve, see Formula 3.

$$Degree\,of\,Sintering\;(DoS) = \frac{\sum a_i}{360°} \tag{3}$$

This is also visualized in Fig. 3 according to [9]. In this example, the angles α_1 and α_2 represent the sufficiently sintered sections leading to a Degree of Sintering of approx. 35 %.

Additionally, selected samples were gold-vaporized and analyzed using scanning electron (SEM) microscopy in combination with X-ray spectroscopy (EDX) in a LEO 1430 P (Carl Zeiss AG, Jena, Germany).

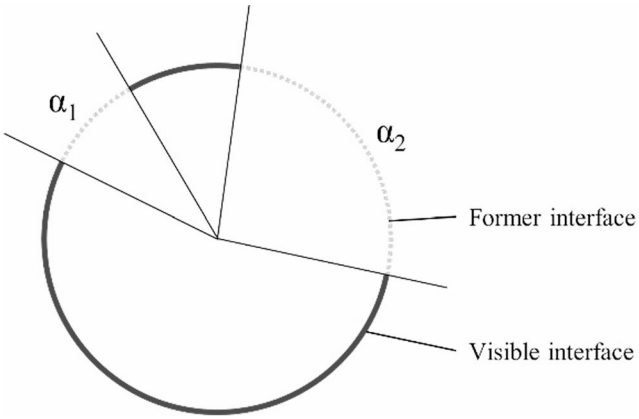

Fig. 3 Schematic visualization of Degree of Sintering for a circular interface [9]

3 Results and discussion

3.1 Dilatometric measurements

The relative length change $\Delta L/L_0$ of Al_2O_3 brown parts with different volume fractions is shown in Fig. 4, where ΔL represents the absolute length change and L_0 the initial specimen length before measurement.

During heating, the length of the specimens increases up to approximately 1100 °C due to thermal expansion. The relative length increase is largely independent of the Al_2O_3 volume fraction in the slurry and corresponds to the expected value of about 0.9 %, based on the thermal expansion coefficient α of 8.4×10^{-6} K^{-1} and a temperature increase of nearly 1100 K. Above 1100 °C, once the onset sintering temperature is exceeded, significant volumetric shrinkage occurs due to the sintering process.

It is evident that as the temperature increases further, the specimen starts to shrink, and at the maximum possible dilatometer temperature of 1650 °C, the sintering process is not yet complete. Specimens with a lower ceramic filler content in the slurry exhibit the expected higher volumetric shrinkage compared to those with a higher ceramic content. The volumetric shrinkage of low-ceramic-content specimens remains significant during the dwell period, whereas those with the highest ceramic content show significantly less shrinkage. Densities of approximately 95 % were achieved for specimens with 40 % Al_2O_3 volume fraction and over 97 % for specimens with 56 % Al_2O_3 volume fraction.

In Fig. 5, the relative length change $\Delta L/L_0$ of green parts of different materials is shown.

The curves indicate that zirconia exhibits significant volumetric shrinkage starting at approximately 1200 °C. By 1650 °C, shrinkage is nearly complete before the dwell time begins, suggesting a temperature delay due to continuous heating. For the composites ATZ, AZ50, and ZTA, shrinkage occurs at a higher temperature than expected due to mutual interference between Al_2O_3 and ZrO_2 during sintering. At the end of the measurement period, all specimens exhibit comparable shrinkage levels, with ZrO_2 showing the highest and AZ50 the lowest shrinkage.

3.2 Real oven process

The results of the density and the hardness of samples sintered with different temperature profiles are shown in Fig. 6.

The results demonstrate that zirconia and the predominantly zirconia-based ATZ exhibit the highest relative densities and hardness values at lower sintering temperatures and shorter dwell times. For dwell times of 2 h (see Fig. 6a) and c)), an increase in sintering temperature appears to have only a limited negative impact on properties, whereas sintering at 1700 °C with a 4 h dwell time significantly reduces hardness.

Conversely, higher sintering temperatures and, to some extent, longer sintering times lead to improved properties for alumina and the predominantly alumina-based ZTA. A sintering temperature of 1650 °C is required for both materials to

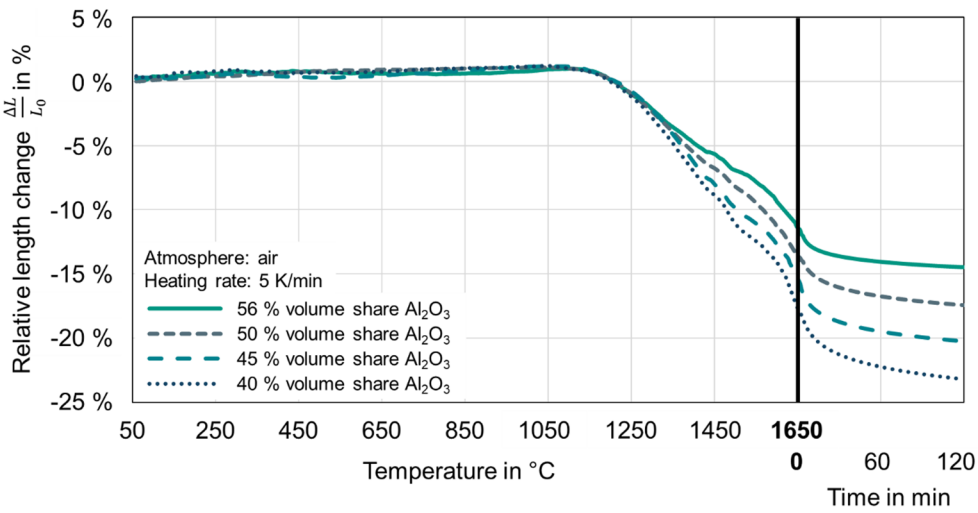

Fig. 4 Dilatometric analysis of Al_2O_3 brown parts with different filler contents

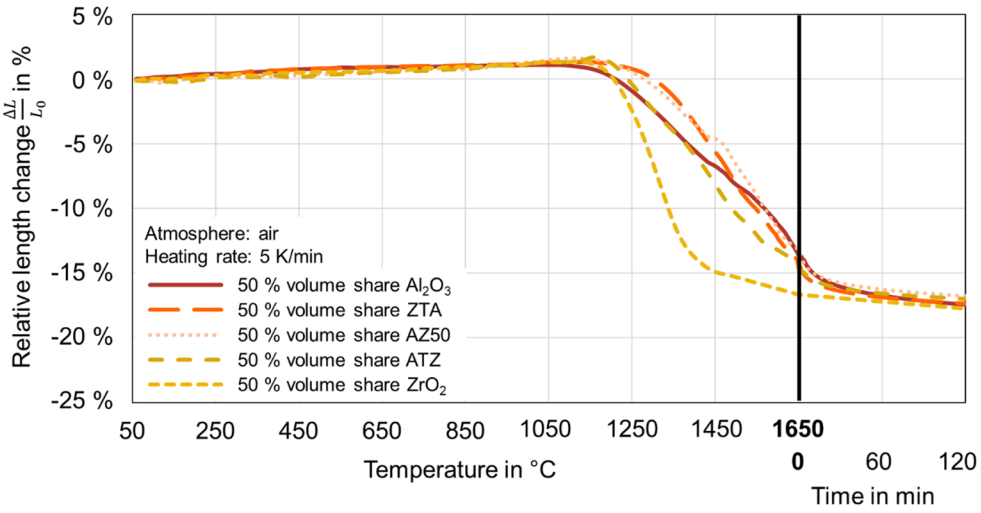

Fig. 5 Dilatometric analysis of components made of slurries with 50 % volume fraction of different ceramic materials

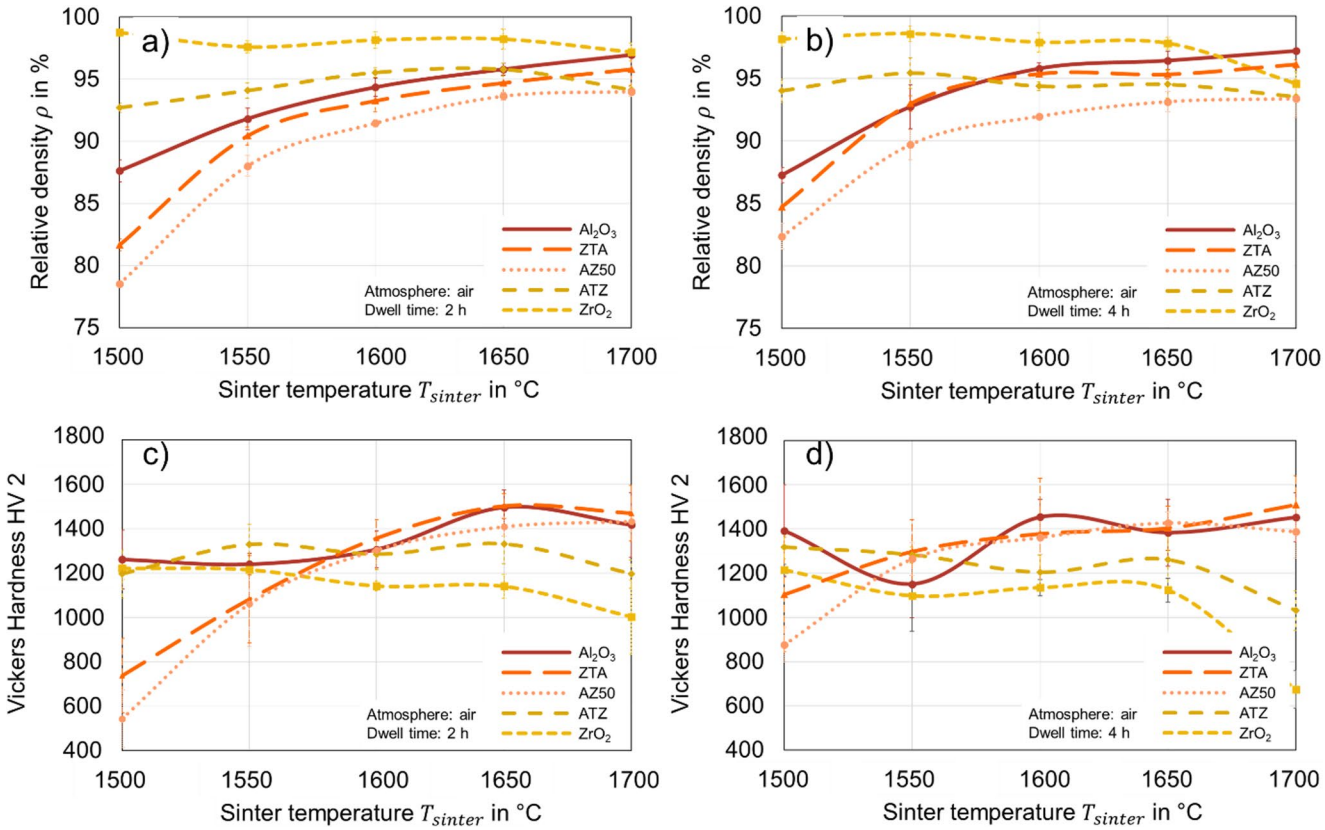

Fig. 6 (**a**) and (**b**) relative density and (**c**) and (**d**) Vickers hardness of samples of various ceramic materials after sintering at different temperatures for 2 and 4 h respectively

achieve sufficient densities of approximately 95 %. Notably, AZ50, which consists of equal mass fractions of Al_2O_3 and ZrO_2, achieves relatively low densities at the same temperature and requires comparatively high temperatures to reach correspondingly high densities. Similar effects were observed by [24] in a nearly eutectic composition of the Al_2O_3 – ZrO_2 system with a 35 % molar ZrO_2 fraction (approximately 46 % by mass), despite employing a different process - directed-energy deposition - which inherently resulted in slightly higher densities [25]. This phenomenon may be attributed to mutual interference between Al_2O_3 and ZrO_2 during sintering, which is more pronounced in compositions with equal proportions of both materials than in compositions dominated by either Al_2O_3 or ZrO_2. As expected, the hardness of alumina

Table 6 Time-temperature-profile derived for sintering the components

Heating time in hh: mm	Heating rate in K/min	Target temperature in °C	Dwell time in h
		25	
00:58	1.3	100	0.0
08:20	2.0	1100	0.0
09:10	1.0	1650	2.0
09:10	−1.0	1100	0.0
08:58	−2.0	25	0.0
	Overall time in h		**38.7**

and ZTA is higher than that of zirconia and ATZ. The hardness values obtained are somewhat lower but still comparable to values reported in relevant literature (e.g [26]). However, due to differences in fabrication and measurement techniques, a direct comparison of the results is limited. When considering all five investigated materials, a sintering temperature of 1650 °C with a dwell time of 2 h appears to yield the best overall properties of the ceramic materials. Furthermore, complementary reference experiments conducted under otherwise identical conditions but using nitrogen as the sintering atmosphere showed that comparable properties could be achieved relative to sintering in air. This suggests that, in the long term, materials from the Al_2O_3 – ZrO_2 system could potentially be combined with ceramics typically sintered in a nitrogen atmosphere.

Based on the above results and also reference profiles from the state of the art, for example [17], the temperature profile applicable for sintering the components was derived, shown in Table 6; Fig. 7. The selected sintering parameters represent a necessary compromise to enable co-sintering of all investigated materials with the same parameters in this basic study. It is acknowledged that such conditions cannot be optimal for each individual ceramic, and may, for instance, lead to excessive grain growth or reduced strength in ZrO_2-based compositions, diminishing the actual properties for some materials. As this study aims to provide a fundamental basis for multi-material sinter joining, uniform parameters were deliberately applied to ensure comparability. In future work, tailored sintering profiles for specific material clusters or just material pairings may allow further optimization of the individual constituent properties.

This temperature profile was also used for sintering the samples of the different materials for B3B analysis. The results obtained are shown in Fig. 8.

The results indicate that AZ50 exhibits the highest flexural strength, while zirconia shows the lowest. As illustrated in Fig. 8b), the manufacturing and sintering process for

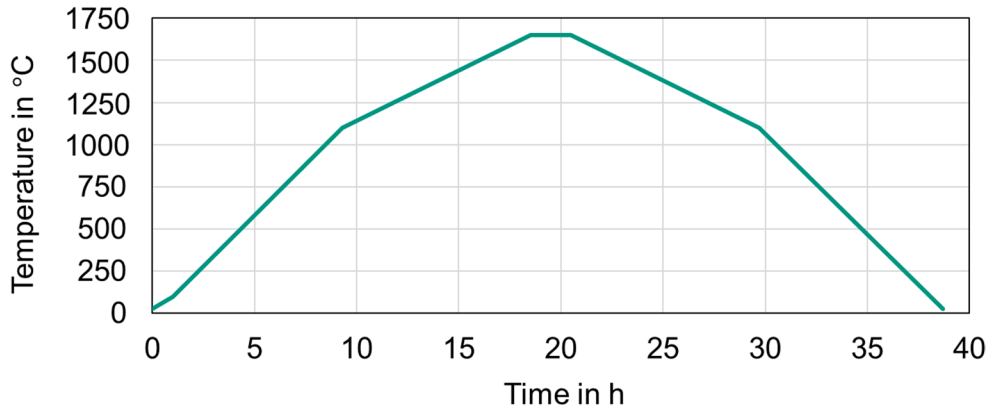

Fig. 7 Time-temperature-profile derived for sintering the components

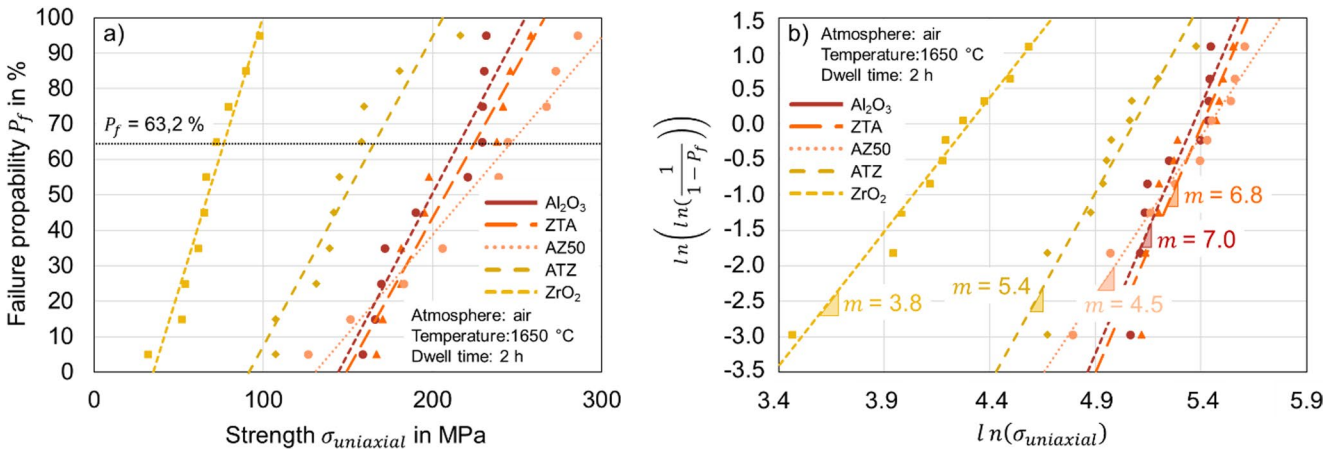

Fig. 8 (**a**) characteristic strength and (**b**) Weibull modulus of samples of various materials sintered at 1650 °C for 2 h in air

alumina and ZTA lead to the most reproducible results due to their high Weibull moduli, whereas zirconia exhibits the least reproducible results due to its low Weibull modulus.

Due to different test setups, preparation methods and special sample sizes (see for example [27]) the quantitative results of the B3B tests can only be compared with literature data to a limited extent. However, the relatively low strength values of ZrO_2 and ATZ compared to the other materials can be attributed to deviations from optimal sintering conditions, leading to excessive grain growth and, consequently, reduced strength (compare for example [28]). The results further show that AZ50 samples sintered at 1650 °C for 2 h exhibit higher strength than Al_2O_3 samples. At the same time, Al_2O_3 specimens display higher hardness compared to AZ50, suggesting that a combination of both materials could potentially lead to advantageous component properties. This difference is likely related to microstructural factors, where AZ50 exhibits a finer-grained due to a hindered grain-growth caused by the mixture of Al_2O_3 and ZrO_2, leading to a more homogeneous matrix and consequently, enhancing the strength. On the other hand, Al_2O_3 forms a denser and more rigid microstructure, resulting in higher hardness but lower fracture toughness.

3.3 Monolithic sinterjoining

The results of the compatibility of cylinders and sleeves of different volume shrinkage are shown in Table 7.

For nominal gaps larger 0.12 mm in the green state, insertion is possible, and for nominal gaps larger 0.32 mm, practically force-free insertion is achievable regardless of the filler content. Increasing the filler content has been shown to enable force-free joining even at smaller gaps. Subsequent measurements after debinding show that components undergo slight shrinkage due to debinding and brief heating to 1100 °C, with greater shrinkage observed at lower filler content. The insertion process is reproducible possible for gaps larger than 20 µm.

After matching cylinders and sleeves, the samples were sintered in a nested configuration at a temperature of 1650 °C for 2 h according to the temperature profile shown in Table 8. The Degrees of Sintering (DoS) obtained after metallographic preparation are summarized in Table 8.

The Degree of Sintering increases independently of the filler content with decreasing inner diameter of the sleeves. The highest DoS occur in the limit range, where it is just possible to match cylinder and sleeve. Radial cracks, initiated at the outer periphery of the sleeves, are particularly evident in sleeves with a ceramic content of 40 % by volume. These cracks are attributed to excessive stresses during the shrinkage process, primarily caused by hoop stresses developing in the sleeve due to the constrained shrinkage of the cylinder during sintering. When the cylinder is showing a significantly lower shrinkage behavior compared to the sleeve, the sleeve is mechanically restricted, generating tensile stresses at its outer periphery, which can exceed the fracture strength of the brittle ceramic material. This stress

Table 7 Compatibility of debinded cylinders and sleeves with different dimensions and filler contents

Cylinder (debinded): 56 % volume share Al_2O_3		Sleeve (debinded): various volume shares Al_2O_3		
		50 %	45 %	40 %
Inner diameter of the sleeve (green state)	5.00 mm	(2)	(3)	(3)
	5.04 mm	(2)	(3)	(3)
	5.08 mm	(2)	(2)	(3)
	5.12 mm	(2)	(2)	(2)
	5.16 mm	(2)	(2)	(2)
	5.24 mm	(1)	(1)	(2)
	5.32 mm	(1)	(1)	(1)
	5.40 mm	(1)	(1)	(1)
	5.48 mm	(1)	(1)	(1)
	5.56 mm	(1)	(1)	(1)
	5.64 mm	(1)	(1)	(1)
	5.72 mm	(1)	(1)	(1)
	5.80 mm	(1)	(1)	(1)
	5.88 mm	(1)	(1)	(1)

Matching: (1) due to the weight force, (2) due to low manual joining force or (3) not possible

Table 8 Degree of sintering for each combination of cylinders and sleeves in %

Cylinder (debinded): 56 % volume share Al_2O_3		Sleeve (debinded): various volume shares Al_2O_3		
		50 %	45 %	40 %
Inner diameter of the sleeve (green state)	5.00 mm	99	-	-
	5.04 mm	99	-	-
	5.08 mm	91	99	-
	5.12 mm	79	100	98
	5.16 mm	55	97	96
	5.24 mm	48	96	94
	5.32 mm	21	76	86
	5.40 mm	17	56	78
	5.48 mm	6	47	63
	5.56 mm	0	38	61
	5.64 mm	0	8	60
	5.72 mm	0	6	43
	5.80 mm	0	6	13
	5.88 mm	0	5	7

state explains the preferential initiation of cracks at the outer sleeve. Accordingly – at least for the selected parameter combinations – the possibility of matching cylinders and sleeves with a small gap does not appear to be a sufficient criterion for the production of defect-free components.

To produce defect-free sintered components, it is essential to consider the temperature-dependent shrinkage behavior in addition to the overall volume shrinkage. Additionally, a small clearance between cylinders and sleeves in matching state, i.e. the brown state, is desired. It is noteworthy that high degrees of sintering can be achieved with all the filler contents of the sleeves considered. Conversely, sleeves with a reduced filler content, when employed in conjunction with highly filled cylinders, exhibit an increased probability for defects. The existence of significant disparities in filler content between the cylinder and sleeves gives rise to uncertainties with regard to shrinkage during the debinding process and the resultant fit during insertion. In the absence of defects, minor discrepancies in filler content are generally preferable.

In order to illustrate the dependencies that occur during the process of sinterjoining, it is necessary to introduce a dimensioning factor $j_{sinterjoining}$, as described in Formula (4). The numerator of this factor considers the ratio of the inner diameter of the sleeve $d_{sleeve,\ inner}$ to the outer diameter of the cylinder $d_{cylinder,\ outer}$, as a measure of the initial relative gap between the cylinder and the sleeve that must be bridged during sintering. The denominator represents the difference in solid loading, i.e. the volume fractions of ceramic material in the parts, between the cylinder $\phi_{cylinder}$ and sleeve ϕ_{sleeve}, which reflects the different shrinkage behaviors of both components and thus, the hypothetical gap that can be closed during sintering.

$$j_{sinterjoining} = \frac{\frac{d_{sleeve,\ inner}}{d_{cylinder,\ outer}}}{\phi_{\ cylinder} - \phi_{\ sleeve}} \tag{4}$$

It has been determined that when factors $j_{sinterjoining}$ are situated between 0.15 and 0.25, a high Degree of Sintering can be accomplished. This is indicative of sufficiently large joint gaps and adequate volume shrinkage.

3.4 Multi-material sinterjoining

Based on the results described above, eleven different combinations of materials of the system Al_2O_3 – ZrO_2 and filler contents were identified. Here, particular attention was paid to ensuring that the components have different material properties for technical applications as well as sufficiently similar sintering behavior, especially in regarding the volume shrinkage over temperature. Analogous to monolithic sinterjoining, the components were co-sintered at 1650 °C for 2 h and analyzed metallographically. The best defect-free combinations of cylinders and sleeves obtained for each material combination are summarized in Table 9.

It is evident that combination 1, combination 6, and combination 7, lead to the highest degrees of sintering. In combination 2, the significant difference in filler content between the cylinder and the sleeve necessitates a large gap in the green body. Smaller gaps lead to cracks in the sleeve, especially starting from the outside periphery. In combinations 3 and 4, none of the examined cylinder-sleeve configurations result in a material bond. Either a circumferential gap remains between the cylinder and the sleeve, or the sleeve is damaged due to shrink-fitting. The same behavior is observed in combinations 8 and 9. A finer gradation of dimensions might enable a bonded joint; however, such a narrow process window would be impractical for potential applications.

Despite having the same nominal filler content, partial sintering is observed in combinations 5 and 11. This is likely

Table 9 Summary of the selected material combinations and their sleeve dimensions of the highest degree of sintering without defects

Combination #	Cylinder	Sleeve	$d_{Sleeve,inner}$	DoS
1	Al_2O_3 56 %	AZ50 50 %	5.12 mm	100 %
2	Al_2O_3 56 %	AZ50 45 %	5.56 mm	71 %
3	Al_2O_3 56 %	ZrO_2 45 %	-	-
4	Al_2O_3 45 %	ZrO_2 40 %	-	-
5	Al_2O_3 50 %	ATZ 45 %	5.48 mm	49 %
6	ZTA 50 %	AZ50 50 %	5.04 mm	98 %
7	ZTA 50 %	ATZ 45 %	5.16 mm	95 %
8	ZTA 50 %	ZrO_2 45 %	-	-
9	ZTA 50 %	ZrO_2 40 %	-	-
10	AZ50 50 %	ZrO_2 45 %	5.12 mm	74 %
11	ATZ 45 %	ZrO_2 45 %	5.32 mm	46 %

due to at least partial contact between the cylinder and the sleeve during the sintering process. Additionally, the greater shrinkage of ZrO_2 during cooling may enhance the bonding, especially if the sintering behavior of the cylinder and sleeve mutually influenced each other.

The factor $j_{sinterjoining}$, introduced for monolithic sinterjoining, does not appear to be directly transferable to multi-material sintering, despite the almost identical absolute shrinkage values of the individual materials at the same filler content. This is mainly due to differences in the temperature-dependent shrinkage evolution and the shrinkage that already occurring during debinding. The latter effect is particularly relevant for ZrO_2, which shows the earliest onset of sintering activity among the materials considered. As a result, larger initial gaps between the cylinder and the sleeve are required. Due to this early shrinkage and potential oversintering, the total shrinkage of ZrO_2 during the joint sintering step may be slightly lower. However, this effect is partially compensated by its slightly higher thermal expansion coefficient, which leads to greater shrinkage during the critical cooling phase.

To generalize the applicability of the $j_{sinterjoining}$ factor, future models must incorporate such material-dependent parameters. In particular, the material-specific onset sintering temperatures, sintering kinetics and thermal expansion coefficients should be incorporated into a future model. Furthermore, additional parameters, e.g. the particle size distribution and the specific surface of the ceramic powders influencing the sintering behavior may be considered. Possibly, these factors may also allow the sintering behavior of the materials to be adjusted and to compensate for a mismatch of the materials.

It can be concluded that combining the most dissimilar materials in the Al_2O_3 – ZrO_2 system, namely Al_2O_3 and ZrO_2, results in a very narrow process window. It remains uncertain whether these two materials can be reproducibly joined via sinterjoining. As demonstrated by the high sintering degree between Al_2O_3 and AZ50, similar materials are easier to combine. Referring to the mechanical properties of the materials discussed in Chap. 3.2, the combination of Al_2O_3 and AZ50 appears not only to yield high Degrees of Sintering but also promising mechanical properties. The high hardness of Al_2O_3 combined with the superior strength of AZ50, could be beneficial in applications such as tubes or bearings subjected to abrasive loads on the inner surface, particularly in the configuration used in combination 1.

Light microscopic and scanning electron microscopic images of the combination 1 are shown in Fig. 9.

The optical microscope images in Fig. 9a) and b) show that no gap is present between the two materials. Even the detailed SEM image in Fig. 9c) reveals no separation between the cylinder and the sleeve, confirming the high degree of sintering.

In the SEM image, an EDX analysis was performed to determine the mass distribution at the interface between Al_2O_3 and AZ50. The measurement line is shown in Fig. 10a) and the results are presented in Fig. 10b). The measured values are normalized exclusively to aluminum and zirconium; for clarity, trace elements such as yttrium, which is used to stabilize ZrO_2 have been omitted.

In the nominal Al_2O_3 regime almost exclusively aluminum (i.e., Al_2O_3) is detected. At the interface, a sharp transition in material composition can be observed, with no significant grading. The aluminum content drops to approximately 50% by mass, while the zirconium content rises to about 50%, corresponding to the respective fractions in AZ50. This suggests that no significant material exchange occurs at the interface, although Fig. 10a) shows isolated bright ZrO_2 grains within the Al_2O_3 region, which may have entered this area during sample preparation. A comparison of grain sizes in both regions reveals that the aluminum oxide grains in the Al_2O_3 regime are significantly

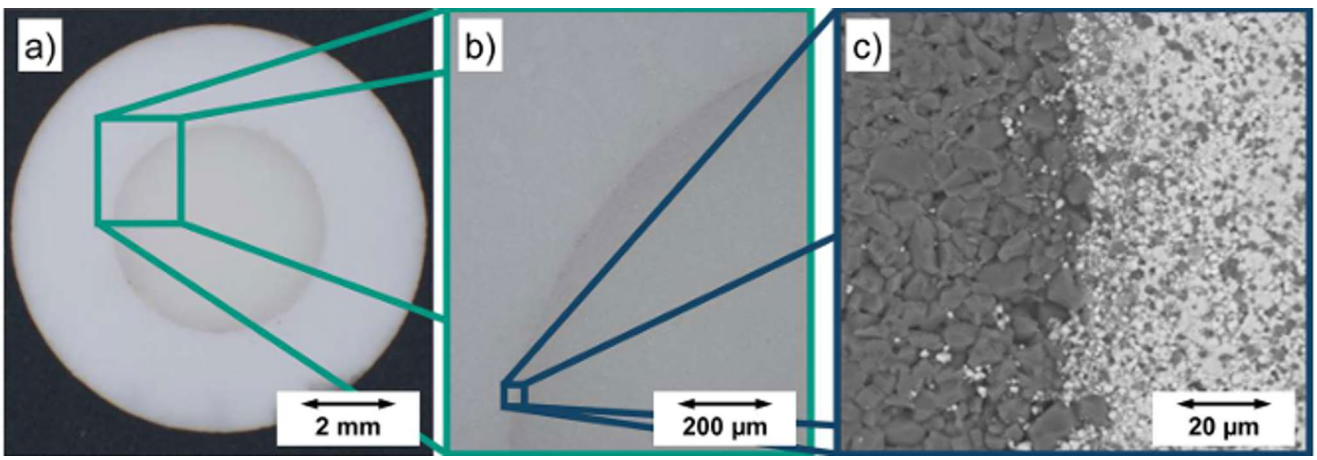

Fig. 9 Material composite according to combination 1 consisting of an Al_2O_3 sleeve (outside) and an AZ50 cylinder (inside) in different magnifications: (**a**) and (**b**) light microscope image, (**c**) SEM image

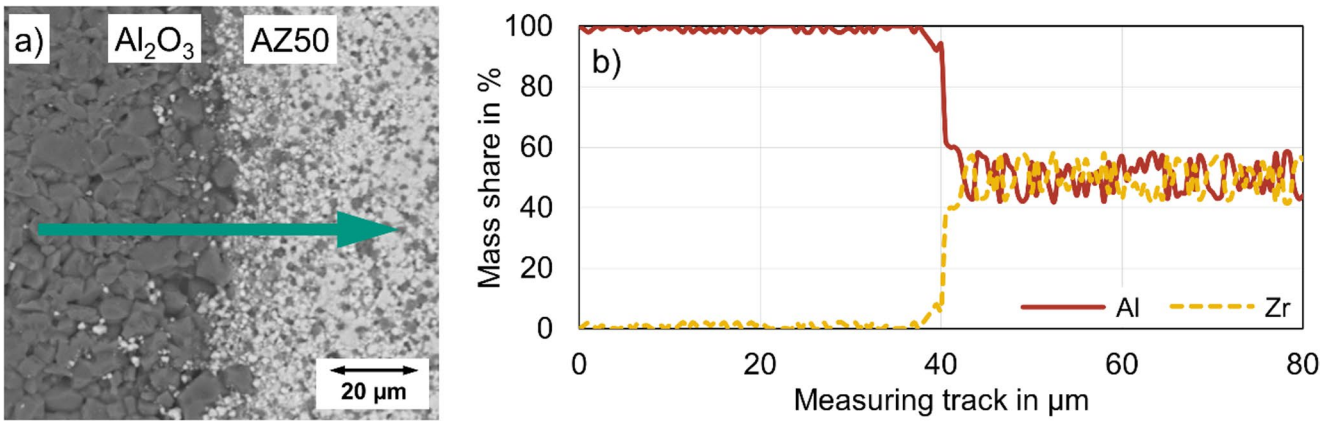

Fig. 10 (**a**) SEM image of the Al_2O_3 – AZ50 interface, (**b**) mass distribution determined by EDX along the line shown in **a**)

larger than those in the AZ50 region. This may be attributed to mutual inhibition of the sintering process between Al_2O_3 and ZrO_2 in the AZ50 regime.

4 Conclusion

In this work, the applicability of a sinterjoining approach to combine different ceramic materials within one component was investigated. First, the shrinkage behavior of different ceramic materials during sintering was examined by dilatometric analysis and sintering conditions applicable for several materials of the material system Al_2O_3 – ZrO_2 were determined. In a first set of experiments, a monolithic sinterjoining approach for combining parts of the same material but different volume shrinkage was investigated. The results were used for a multi-material sinterjoining approach, i.e., the combination of different materials in a single component.

The main findings are:

- With decreasing filler content, the shrinkage of the components during sintering increases.
- The shrinkage behavior of different ceramic materials differs, whereby components made of different materials but with the same filler content show approximately the same shrinkage at the end of the sintering process.
- Sintering conditions of 1650 °C with a holding time of 2 h lead to satisfactory results for various ceramic materials of the system Al_2O_3 – ZrO_2 and therefore, represent a reasonable compromise for co-sintering.
- It is possible to perform successfully a sinterjoining approach of VPP components with different filler contents, both in monolithic and multi-material design.
- For monolithic sinterjoining, a factor $j_{sinterjoining}$ was definded to dimension the inner and outer part based on their filler contents to obtain high Degrees of Sintering.
- Multi-material sinterjoining is significantly more complex. Nevertheless, good results have been achieved for various material combinations. In particular, the combination of Al_2O_3 and AZ50 appears to be promising.

The results of this work demonstrate the potential of combining different materials within one component. They serve as a starting point for further investigations, especially regarding a transfer to real components. There, the advantages of the multi-material design can be used in a specific manner. In addition, the results can also be used in multi-material VPP to enhance the interface between the materials. A next step for future work will be identifying optimized parameter combinations in a narrower scope based on the results of the present work, e.g. for smaller material clusters or just material pairs, allowing a best matching compromise for these materials. Additionally, a key next step is a quantitative mechanical characterization of the joint interfaces, allowing a directly link of process parameters and microstructural properties to the functional performance, which also enables quantification of the potential of multi-material design.

Acknowledgements The authors thank Lena Mohs and especially Alina Wehrle for performing the experiments regarding the influence of the sintering conditions on the material properties. Furthermore, the authors thank the Institute of Applied Materials - Ceramic materials and technologies, and especially Dominic Creek, for the support in performing the B3B tests.

Author contributions Johannes Schubert: Conceptualization, Formal Analysis, Investigations, Methodology, Project Administration, Validation, Visualization, Writing - Original Draft, Writing - Review & Editing ||| Michael Schott: Data Curation, Formal Analysis, Investigations, Methodology, Validation, Writing - Original Draft ||| Frederik Zanger: Conceptualization, Funding Acquisition, Resources, Supervision, Validation, Writing - Review & Editing.

Funding Open Access funding enabled and organized by Projekt DEAL.

Data availability No datasets were generated or analysed during the current study.

Declarations

Competing interests The authors declare no competing interests.

References

1. Chaudhary RP, Ahmad F, Yasin T, Jamil T, Choi J-P (2022) Additive manufacturing of polymer-derived ceramics: materials, technologies, properties and potential applications. Prog Mater Sci 128:100969. https://doi.org/10.1016/j.pmatsci.2022.100969
2. Lakhdar Y, Tuck C, Binner J, Terry A, Goodridge R (2021) Additive manufacturing of advanced ceramic materials. Prog Mater Sci 116:100736. https://doi.org/10.1016/j.pmatsci.2020.100736
3. Nazir A, Abate KM, Kumar A, Jeng JY (2023) Multi-material additive manufacturing: a systematic review of design, properties, applications, challenges, and 3D printing of materials and cellular metamaterials. Mater Des 226:111661. https://doi.org/10.1016/j.matdes.2023.111661
4. Schwarzer-Fischer E, Winkler R, Horny N, Janek M, Mülhaupt L, Schubert J (2022) Study on CerAMfacturing of novel alumina aerospike nozzles by lithography-based ceramic vat photopolymerization (CerAM VPP). Materials 15(9):93279. https://doi.org/10.3390/ma15093279
5. Homa J, Schwentenwein M (2014) A Novel Additive Manufacturing Technology for High-Performance Ceramics. In: Reithmaier JP, Haisma J, Lee C, Pavesi L (eds) Advanced Processing and Manufacturing Technologies for Nanostructured and Multifunctional Materials. Wiley, pp 33–40. https://doi.org/10.1002/9781119040354.ch4
6. Zakeri S, Vippola M, Levänen E (2020) A comprehensive review of the photopolymerization of ceramic resins used in stereolithography. Additive Manuf 35:101177. https://doi.org/10.1016/j.addma.2020.101177
7. Michaelis A, Kern F, Stöcker B, Felden J, Koch D, Krause M (2020) Advanced manufacturing for advanced ceramics. Procedia CIRP 95:18–22. https://doi.org/10.1016/j.procir.2020.11.002
8. Schubert J, Lehmann C-L, Zanger F (2024) Versatile binder system as enabler for multi-material additive manufacturing of ceramics by vat photopolymerization. Ceram Int 50(23B):50948–50954. https://doi.org/10.1016/j.ceramint.2024.10.006
9. Schubert J, End Y, Schulze V, Zanger F (2022) Exploring the applicability of sinterjoining to combine additively manufactured ceramic components. Procedia CIRP 115:18–23. https://doi.org/10.1016/j.procir.2022.10.043
10. Klimscha K (2014) Einfluss des Fügespalts auf die erreichbare Verbindungsqualität beim Sinterfügen. Dissertation, Karlsruher Institut für Technologie. Shaker, Aachen. ISBN: 978-3-8440-2628-3
11. Ruh A, Dieckmann A-M, Heldele R, Piotter V, Ruprecht R, Munzinger C, Fleischer J, Haußelt J (2008) Production of two-material micro-assemblies by two-component powder injection molding and sinter-joining. Microsyst Technol 14:1805–1811. https://doi.org/10.1007/s00542-008-0646-8
12. Ruh A, Piotter V, Plewa K, Ritzhaupt-Kleissl H-J, Haußelt J (2011) Influence and limits of sintering temperatures on the movability of shaft-to-collar connections formed by two-component micro powder injection moulding. Microsyst Technol 17:1541–1546. https://doi.org/10.1007/s00542-011-1324-9
13. Schwarzer-Fischer E, Abel J, Müller F, Rebenklau L, Barth H, Alsdorf N, Weingarten S, Scheithauer U, Zins M (2021) Marriage of technologies – hybridization of materials and manufacturing technologies for ceramic components. cfi/Ber DKG 98:E39–E45
14. ISO 13320 2020 Particle size analysis — Laser diffraction method
15. ISO 9277 2022 Determination of the specific surface area of solids by gas adsorption — BET
16. ISO 21821: 2019 Fine ceramics (advanced ceramics, advanced technical ceramics) – Determination of densification properties of ceramic powders on natural sintering
17. Lithoz GmbH (2020) Thermal Post Processing – LithaLox 350 – Technical Data Sheet
18. ISO 18754 (2020) Fine ceramics (advanced ceramics, advanced technical ceramics) – Determination of density and apparent porosity
19. ISO 14705:2016 Fine ceramics (advanced ceramics, advanced technical ceramics) – Test method for hardness of monolithic ceramics at room temperature
20. Börger A, Supancic P, Danzer R (2002) The ball on three balls test for strength testing of brittle discs: stress distribution in the disc. J Eur Ceram Soc 22(9):1425–1436. https://doi.org/10.1016/S0955-2219(01)00458-7
21. Börger A, Supancic P, Danzer R (2004) The ball on three balls test for strength testing of brittle discs: part II: analysis of possible errors in the strength determination. J Eur Ceram Soc 24(10):2917–2928. https://doi.org/10.1016/j.jeurceramsoc.2003.10.035
22. Danzer R, Börger A, Supancic P, Ruiz Villanueva MA (2003) Ein einfacher Festigkeitsversuch für scheiben Aus spröden werkstoffen. Materialwiss Werksttech 34(5):490–498. https://doi.org/10.1002/mawe.200390098
23. ISO 20501 2019 Fine ceramics (advanced ceramics, advanced technical ceramics) – Weibull statistics for strength data
24. Wu Y-R, Guo S-Y, Zhang C-H, Zhang X-J, Li L-J, Liu Y-P, Zhao Z, Liu Y-G (2023) Influence of the content of polymethyl methacrylate on the properties of porous Si3N4 ceramics fabricated by digital light processing. Ceram Int 49(19):31228–31235. https://doi.org/10.1016/j.ceramint.2023.07.070
25. Wu D, San J, Niu F, Zhao D, Huang Y, Ma G (2020) Directed laser deposition of Al2O3–ZrO2 melt-grown composite ceramics with multiple composition ratios. J Mater Sci 55(16):6794–6809. https://doi.org/10.1007/s10853-020-04524-7
26. Lithoz GmbH (2025) Materials. https://www.lithoz.com/en/materials/materialoverview/. Accessed 03 Sept 2025
27. Harrer W, Danzer R, Supancic P, Lube T (2007) The Ball on Three Balls Test: Strength Testing of Specimens of Different Sizes and Geometries. In: Heinrich JG, Aneziris C (eds) Proc 10th Int Conf Eur Ceram Soc, June 17–21, 2007, Berlin, Germany. Göller, Baden-Baden
28. Kang S-JL (2004) Sintering: Densification, Grain Growth and Microstructure. Elsevier. ISBN: 978-0-08-049307-7